

Deep Fusion of Intrinsic Vibration Information and Grassmann Manifold-based Similarity for Fault Identification of Reciprocating Compressor

Ying Zhang^a, Jinchen Ji^{b,*}, Xiaowang Chen^a

^a*School of Mechanical Engineering, University of Science and Technology Beijing, Beijing 100083, China*

^b*School of Mechanical and Mechatronic Engineering, University of Technology Sydney, Ultimo, NSW 2007, Australia*

Abstract

This paper introduces a new method based on deep belief networks (DBN) to integrate intrinsic vibration information and assess the similarity of subspaces established on the Grassmann manifold for intelligent fault diagnosis of a reciprocating compressor (RC). Initially, raw vibration signals undergo empirical mode decomposition (EMD) to break them down into multiple intrinsic mode functions (IMFs). This operation can reveal inherent vibration patterns of fault and other components hidden in the original signals. Subsequently, features are refined from all the IMFs and concatenated into a high-dimensional representative vector, offering localized and comprehensive insights into RC operation. Through DBN, the fault-sensitive information are further refined from the features to enhance their performance in fault identification. Finally, similarities among subspaces on the Grassmann manifold are computed to match fault types. The efficacy of the method is validated using field data. Comparative analysis with traditional approaches for feature dimension reduction, feature extraction, and Euclidean distance-based fault identification underscores the effectiveness and superiority of the proposed method in RC fault diagnosis.

Keywords: Fault diagnosis, Reciprocating compressor, Intrinsic vibration, Grassmann manifold, Deep belief network, Empirical mode decomposition

1. Introduction

Reciprocating compressors (RCs) are widely used in industrial manufacturing. A continuous and stable operation of RCs is crucial to guarantee the high-efficient production. However, once fault or failure occurs in a certain part of RC, the machinery will operate irregularly or even break down, which may lead to serious economic loss to the factories or companies. Therefore, it is crucial to monitor the health condition of RC and reduce the costly downtime [1].

With the advent of the Internet of Things and wireless transmission [2], there has been an exponential increase in the volume of data acquired for monitoring the operating condition of RC systems. This burgeoning amount of data presents both a challenge and an opportunity [3]. On the one hand, it contains a wealth of potentially useful information indicative of machine health; on the other hand, it may harbor hidden patterns and regularities that are not easily discernible by human observers [4]. Consequently, the task of extracting reliable information from big data and enhancing the accuracy of fault diagnosis has emerged as a significant challenge in the field of condition monitoring [5]. Conventional fault identification methods typically extract one or several features from the time and/or frequency domain of original signals [6], then employ shallow models such as principle component analysis [7] for feature fusion and dimension reduction. While these approaches demonstrate good performance in fault identification, they suffer from three key limitations: (1) Traditional methods may not fully exploit the rich and local information embedded in the vibration signals, leading to suboptimal feature representation and reduced diagnostic accuracy. Vibration signals often contain important information at multiple scales, ranging from high-frequency details to low-frequency trends.

*Corresponding author

School of Mechanical and Mechatronic Engineering, University of Technology Sydney, Ultimo, NSW 2007, Australia
Email: Jin.Ji@uts.edu.au

Traditional methods may not effectively capture this multiscale information, leading to an incomplete representation of the signal's characteristics. (2) The high-dimensional nature of extracted features can introduce redundancy, making it difficult to efficiently and accurately process the data for fault diagnosis. Traditional methods use shallow model structures to fuse feature, which make the noise information cannot be removed effectively. Shallow models do not provide the hierarchical feature representation needed to capture multiple levels of abstraction in the data. This can lead to a loss of important information, reducing the ability to identify subtle fault characteristics. (3) Current methods are typically based on linear assumptions or simplified models that do not adequately capture the complex, nonlinear relationships inherent in RC data [8]. However, actual RC systems exhibit highly nonlinear behavior due to factors like varying load conditions, wear and dynamic interactions between components. Linear models can fail to account for these complexities, resulting in an incomplete understanding of the RC system's behavior, which leads to the limited handling of nonlinearities of RC signals. To address these challenges, this paper focuses on three key aspects for research development.

To extract more local and subtle information, the vibration signal can be decomposed into sub-modal signal, each representing a distinct oscillatory pattern. This decomposition captures localized and intrinsic oscillations and provides a detailed representation of the signal at multiple scales. Wavelet transformation has gained great success in sub-mode extraction from different scales of signal [9]. However, base functions need to be selected by expertise before signal decomposition. Inappropriate selections would select the incorrect scale information and degrade the fault diagnosis performance. To alleviate this drawback, Niu et al. developed a novel method based on EMD for fault diagnosis. Vibration signal is decomposed into several components by EMD to highlight the local information [10]. Li et al. used an EMD-based method to decompose the load into different frequency components changing from low to high levels [11]. The EMD method can decompose signals self-adaptively without the assistance of prior knowledge [12]. It can emphasize the local frequency information from different scales of signal. Therefore, EMD is employed to break down the original monitoring signals of the RC into a collection of IMFs. These intrinsic functions aptly capture the inherent vibrations of the RC from localized perspectives. It provides a more confident representation of its operating conditions and reflects the underlying dynamics of the system, including non-stationary and transient behaviors.

To comprehensively capture useful information from intrinsic vibrations, a multitude of features were extracted from each IMF. These features were then utilized to construct a high-dimensional vector, enabling a thorough representation of the RC operating conditions [13]. However, high-dimensional feature vectors often contain a significant amount of redundant information. Multiple features may reflect similar characteristics of the signal, leading to the overlap and redundancy of information. This increases not only the computational complexity but also difficulty in identifying the most relevant features for fault diagnosis. Moreover, in the intricate operation environment, RC vibration signals are susceptible to other fault-irrelative contamination. Thus, dimension reduction techniques are essential to eliminate such redundancy of feature vectors and further bolster the performance of fault diagnosis. Traditionally, feature dimension reduction in RC fault diagnosis has been achieved through methods such as principal component analysis (PCA) [7] and kernel principal component analysis (KPCA) [14]. These techniques extract essential information from raw signals using linear or non-linear matrix transformations. However, given the scale of big data in RC fault diagnosis, these approaches may not suffice. Therefore, there is a growing interest in exploring more robust methods for feature dimension reduction. Deep learning methods have gained traction in academic circles due to their ability to perform feature fusion in depth [15, 16]. DBNs can fuse high-dimensional features into a lower-dimensional, deeply-fused feature vector. The multi-layer architecture of DBNs enables the extraction of hierarchical features that capture complex, nonlinear relationships within the data by considering mutual information of neighboring layers [17, 18]. Thus it preserves essential information and improving diagnostic accuracy of RC.

After the features are deeply fused, pattern recognition method need to be selected to automatically assign the fault types. Currently, most fault identification methods either depend on Euclidean distance [19] or make assumptions about data following certain distributions[20]. Given that RC vibration signals are both nonlinear and non-stationary [21], such an assumption could be unreasonable. It could overlook crucial nonlinear information and thereby compromising the fault diagnosis performance. To address this issue, this paper devises a similarity metric based on GM for RC fault diagnosis. GM comprises a set of subspaces capable of representing the operating conditions of the RC [22].

The lower-dimensional feature vector is mapped onto subspaces on the Grassmann manifold. This approach ensures that the most informative and nuanced features are retained. The Grassmann manifold provides a geometric

framework that captures the intrinsic structure of the data subspaces, making it well-suited for analyzing complex non-linear fault patterns. The similarity between subspaces of real-time monitoring data and different fault monitoring data on Grassmann manifold can be evaluated using the geodesic distance metric [23]. The use of geodesic distance for comparing subspaces allows for accurate similarity measurement, which is crucial for distinguishing between different fault conditions. This methodology enhances the accuracy of fault diagnosis by retaining essential nonlinear information and reducing sensitivity to noise and variations in the data. Additionally, the Grassmann manifold-based approach is robust to changes in operating conditions, making it highly effective to RC data of real-world industrial applications where data variability is common.

In the quest for intelligent fault diagnosis of reciprocating compressor in the context of big data, this paper presents a hybrid approach that combines EMD, DBN and a Grassmann manifold-based similarity metric. The contributions of this paper can be summarized as follows.

1. This paper present a comprehensive and integrated framework that combines EMD, DBN-based feature fusion, and Grassmann manifold analysis. This holistic approach ensures a more robust and accurate fault diagnosis by leveraging the strengths of each method in a unified manner.
2. EMD is used to extract multi-scale local features to highlight subtle variations in signal. High-dimensional features are extract from each IMF calculated by EMD to reflect the operation condition of RC comprehensively. In contrast to shallow models for feature fusion, this paper employs DBN to achieve deep feature fusion. This approach captures complex, nonlinear relationships within the data, preserves essential information, and enhances the discriminative capability of the feature set.
3. The low-dimensional feature vectors are transformed into subspaces on the Grassmann manifold, where RC faults are identified using the proposed geodesic distance-based similarity. Unlike Euclidean methods, this metric measures the nonlinear similarity on the GM. It retains nuanced nonlinear information and improves the accuracy of fault identification. This geometric approach is robust to data variability and changes in operating conditions.

The paper is structured as follows. Section 2 introduces the developed method and offers a concise overview of related theories. Section 3 examines the experimental data and validate the effectiveness of the proposed approach. Section 4 provides conclusions drawn from the findings presented in this paper.

2. Proposed method

This paper proposes a novel method for intelligent RC fault diagnosis. Recognizing the non-linear and non-stationary nature of RC signals, this paper employs EMD to decompose RC vibration signals into IMFs, obtaining intrinsic fault-related vibrations. From these IMFs, features are extracted to assemble high-dimensional vectors, offering insights into local signal characteristics and working conditions. Subsequently, DBN are leveraged to deeply fuse these features, simultaneously reducing feature vector dimensionality and eliminating redundant information. The deeply fused feature vectors are then transformed into subspaces on the Grassmann manifold, facilitating fault determination through similarity calculations between subspaces. The detailed procedure is depicted in Fig.1 and discussed below.

1. Vibration signals from the RC are gathered utilizing accelerometers strategically mounted on the cylinder. These accelerometers are positioned to precisely capture the vibrations occurring within the cylinder during operation.
2. The measured vibration signals are subjected to decomposition through EMD. This process effectively breaks down the signals into a collection of IMFs, enabling the extraction of inherent fault-related vibrations within the RC system.
3. Features are computed individually from each IMF to capture the distinct operating conditions of the RC from a localized perspective. This method guarantees that the extracted features precisely depict the specific characteristics inherent to each IMF, offering an intricate understanding of the RC behavior.
4. The features extracted from each IMF are amalgamated into a unified high-dimensional feature vector. This feature vector serves as a holistic depiction of the RC operational state, encompassing the diverse aspects captured by the individual features from each IMF.

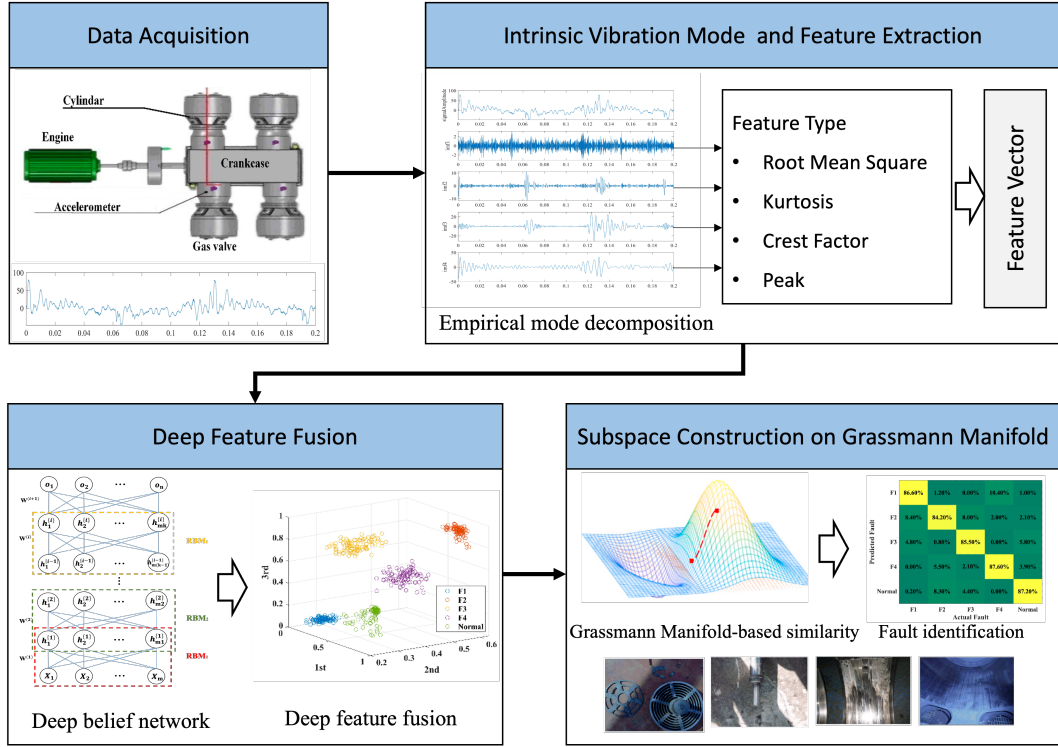


Figure 1: Schematic of the proposed method

5. The feature vectors undergo partitioning into distinct datasets dedicated for training and testing purposes. This separation allows for the utilization of one subset for model training and the other for assessing the model performance.
6. The feature vectors are fed into a DBN to fuse feature and reduce the dimensionality of the feature vectors. This process involves transforming the high-dimensional feature representations into a more compact and informative format, facilitating more efficient analysis and interpretation.
7. The feature vectors extracted from the training data are transformed into subspaces on the Grassmann manifold, with each fault serving as the reference or base subspace. This transformation process facilitates fault identification by aligning the feature vectors with the characteristic subspaces associated with each fault condition.
8. The subspaces for the testing data are computed through an iterative process involving the application of Steps 6 and 7. This iterative procedure ensures that the feature vectors extracted from the testing data are appropriately transformed into subspaces on the Grassmann manifold, allowing for accurate fault identification and diagnosis.
9. To determine the fault type, the similarities between the subspaces representing the testing data and those representing the fault data are calculated. This involves assessing the degree of resemblance or proximity between the subspaces derived from the testing data and the reference subspaces associated with each fault type.

2.1. Empirical mode decomposition

EMD possesses the ability to break down signals into a collection of IMFs [24], with each IMF representing a unique intrinsic vibration mode induced by RC fault excitations. As a result, IMFs provide localized information about the operating conditions, offering a finer resolution of fault-related dynamics. The fundamental steps of EMD are summarized as follows.

1. Compute the upper and lower envelopes of the original signals by identifying the maximum and minimum values within a specified window, respectively. Calculate the mean values of these envelopes, referred to as m_1 .

Table 1: Extracted features

| Feature | Equation | Symbol | Meaning |
|------------------|---|--------|---|
| Root mean square | $X_{RMS} = \sqrt{\frac{\sum_{i=1}^n (x(i))^2}{n}}$ | X_1 | Indicating the average energy of signals |
| Crest factor | $X_{Crest} = \frac{\max\{x(i)\}}{X_{RMS}}$ | X_2 | Indicating the peak amplitude divided by the RMS value |
| Kurtosis | $X_{Kurt} = \frac{\sum_{i=1}^n (x(i) - \bar{x})^4}{n(X_{RMS})^4}$ | X_3 | The fourth standardized moment, representing the shape of a probability distribution and is sensitive to impulsive faults |
| Peak | $X_{Peak} = \max x $ | X_4 | Indicating the intensity of vibration |

- Determine the difference between the raw signals $x(t)$ and the mean m_1 , expressed as the deviation from the mean.

$$x = x(t) - m_1 \quad (1)$$

- The variable x denotes the raw signal used for computing the first IMFs through iterative applications of Steps 1 and 2 for k iterations. The formula for obtaining the first IMF is given as follows.

$$\text{IMF}_1 = x_1 = x_{1(k-1)} - m_{1k} \quad (2)$$

- Repeat the aforementioned three steps until the stop criterion is satisfied, ensuring the computation of all IMFs.
- From the above-mentioned precedures, it can be inferred that

$$x(t) = \sum_{i=1}^I \text{IMF}_i + r \quad (3)$$

where I represents the total number of IMF components, and r signifies the residual component.

2.2. Feature extraction of intrinsic vibration for vector construction

To comprehensively capture the localized operating characteristics of the RC, a set of features is meticulously extracted from each IMF. These features encompass various aspects of the signal dynamics and are succinctly summarized in Table 1. Transient faults often cause brief but significant changes in the signal. The RMS value can help in detecting these transient changes by averaging over time. This makes it possible to identify faults that may not be obvious in a short time-domain inspection. Faults can cause non-stationary behavior in a RC system and cause the non-stationary property of signals. The crest factor can identify such behavior by comparing peak values to the overall energy of the signal. Many types of faults cause impulsive or intermittent events, such as piston rod breaking. These events produce signals with high peaks and heavy tails, leading to high kurtosis. By monitoring kurtosis, these impulsive events can be detected more effectively. The peak value directly captures the highest amplitude excursions in a signal. Faults often manifest as extreme events or bursts of energy that cause the signal to reach unusually high values.

Once features are computed from each IMF, they are assembled into a high-dimensional feature vector. This vector effectively combines the diverse information captured by the individual features from each IMF, providing a comprehensive representation of the RC operational characteristics.

$$X = (X_1, X_2, \dots, X_i, \dots, X_I) \quad (4)$$

In this expression, $X_i = [X_{i1}, X_{i2}, X_{i3}, X_{i4}]$ denotes the concatenated feature vector, wherein each feature is extracted from the i -th IMF as specified in Table 1. These distinct features are combined to construct a high-dimensional feature vector, thereby offering a comprehensive representation of the operating condition.

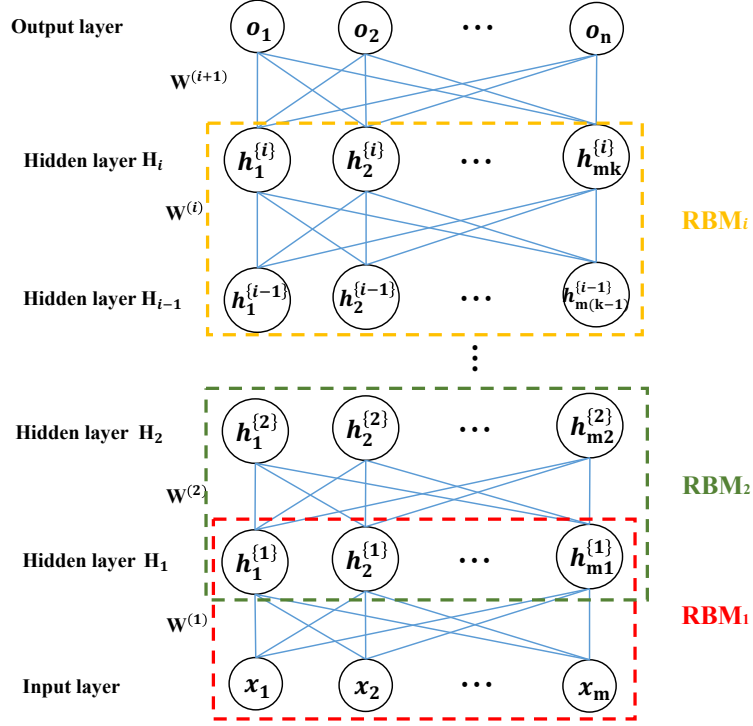


Figure 2: The DBN structure

2.3. Deep feature fusion by deep belief networks

The deep belief network encompasses sophisticated architectures that excel in extracting feature representations from monitoring data. These architectures are adept at revealing intricate patterns and characteristics inherent in the data, facilitating a comprehensive understanding of its underlying complexities [25].

Figure 2 provides an illustration of a standard DBN architecture, delineating its structural components and interconnections. $X = (X_1, X_2, \dots, X_m)$ represents the aggregation of high-dimensional features derived from the IMFs, offering a comprehensive portrayal of the RC operational characteristics. Conversely, $O = (o_1, o_2, \dots, o_n)$ pertains to the deeply fused features computed by the DBN. These features are meticulously engineered to effectively capture fault-sensitive information, thereby facilitating precise fault diagnosis and classification. The DBN comprises i hidden layers, each hosting m_1, m_2, \dots, m_k nodes, respectively. Constructed through a sequence of RBMs, these models learn joint probability distributions of nodes across adjacent layers. Each RBM consists of input and output layers, with nodes within the same layer unconnected, while neighboring layers are interconnected via weight matrices (and biases). The outputs of one RBM serve as inputs for the next RBM in the sequence. The energy of the input can be expressed as

$$E(v, h) = -a^T v - b^T h - v^T W h \quad (5)$$

In Boltzmann machines, the probability distribution governing variables h and/or v is established based on the following energy function

$$P(v, h) = \frac{e^{-E(v, h)}}{Z} \quad (6)$$

where Z is a normalization function.

The marginal probability of a visible vector, with each element represented as a Boolean value, is determined by summing over all potential configurations of the hidden layer. This mathematical expression entails summing the joint probabilities of various combinations of hidden layer states, integrating across the entire range of possible hidden layer configurations.

$$P(v) = \frac{1}{Z} \sum_h e^{-E(v,h)} \quad (7)$$

The probability of an visible unit conditioned on a specific hidden unit in the RBM is calculated by the following equation

$$P(v|h) = \prod_{i=1}^m P(v_i|h) \quad (8)$$

On the other hand, the probability of a hidden node h conditioned on an visible node v can be expressed as

$$P(h|v) = \prod_{j=1}^{mk} P(h_j|v) \quad (9)$$

The probabilities of individual activations can be computed using

$$P(h_j = 1|v) = \sigma \left(b_j + \sum_{i=1}^m w_{ij} v_i \right) \quad (10)$$

$$P(v_i = 1|h) = \sigma \left(a_i + \sum_{j=1}^{mk} w_{ij} h_j \right) \quad (11)$$

where σ denotes the sigmoid function. Additional information on DBN can consult [26].

2.4. Grassmann manifold-based similarity

Following the dimension reduction by DBN, this paper introduces a similarity metric based on the Grassmann manifold for fault type identification. This approach involves the creation of subspaces on the Grassmann manifold, with fault types determined by calculating the geodesic distance of between real-time subspaces and basis subspaces.

Grassmann manifolds (GM) are a type of Riemannian manifold embedded within a high-dimensional Hilbert space [27]. A GM, denoted as $\mathcal{G}_{d,D}$, comprises a set of d -dimensional subspaces of \mathbb{R}^D . These subspaces are spanned by orthonormal matrices Y and are represented as $span(Y)$. Each subspace within the Grassmann manifold encapsulates a distinct configuration of d dimensions within the overarching D -dimensional space. Two deeply-fused feature matrices, O_1 and O_2 , presumed to be derived from DBN, are spanned by Y_1 and $Y_2 \in \mathbb{R}^{D \times d}$, respectively. The similarity between the subspaces $span(Y_1)$ and $span(Y_2)$ is gauged by computing principal angles, which can be determined using

$$\cos \theta_i = \max_{u_i \in span(Y_1)} \max_{v_i \in span(Y_2)} u_i v_i \quad (12)$$

with the following conditions

$$\begin{aligned} u_i' u_i &= v_i' v_i = 1 \\ u_i' u_j &= v_i' v_j = 0 \\ i &= (1, 2, \dots, d) \quad j = (1, 2, \dots, i-1) \end{aligned} \quad (13)$$

where u and v represent the principal vectors of real-time data subspace and fault basis subspace, respectively. To compute the principal angles, singular value decomposition (SVD) is employed [28]. This mathematical technique facilitates the derivation of principal angles, which can be expressed as follows.

$$Y_1' Y_2 = U S V^* \quad (14)$$

where $U = [u_1, u_2, \dots, u_d]$ denotes a unitary matrix representing the principal vectors. $S = [\cos \theta_1, \cos \theta_2, \dots, \cos \theta_d]$ represents a diagonal matrix containing the cosine values of the principal angles. Additionally, V^* signifies the conjugate transpose of the matrix $V = [v_1, v_2, \dots, v_d]$, which contains the principal vectors corresponding to the other

subspace. The similarity between two subspaces on the GM is computed on the basis of a geodesic distance. This is defined as follows.

$$dist(Y_1, Y_2) = \sum_{i=1}^d \cos^2 \theta_i \quad (15)$$

In the scenario where $\theta_1 = \theta_2 = \dots = \theta_d = 0$, indicating that the principal angles between the subspaces are all zero, the two subspaces, e.g., $span(Y_1)$ and $span(Y_2)$, are effectively collapsed into one. When the geodesic distance $dist(Y_1, Y_2)$ is higher and close to one, it suggests a greater similarity between two subspaces. This implies a higher likelihood that the feature matrices O_1 and O_2 fall into the same fault type of RC. In this study, each fault's subspace acts as a reference point and is compared with the subspace of the data being analyzed to assess their similarity. The fault type is subsequently determined by evaluating the computed similarity value. This approach enables the comparison of data subspace with established fault subspace references, thereby enabling precise fault identification based on the observed degree of similarity.

The Grassmann manifold-based similarity considers subspaces rather than individual data points to match the fault type. This approach inherently averages out noise and small variations within the subspaces, making the analysis more robust to random fluctuations and measurement noise. By capturing the entire subspace, this approach inherently includes the variations and interactions within the data, which are often nonlinear. This holistic representation allows for a more comprehensive understanding of the underlying structure of the data, preserving nuances that might be missed when considering points in isolation. By calculating with subspaces, Grassmann manifold methods can capture the global structure of the data. This is particularly useful in fault diagnosis, where the overall pattern and relationships between different variables can be more indicative of faults than individual variable changes. The geodesic distance on the Grassmann manifold is the length of the shortest geodesic path connecting two points (subspaces) on the manifold. This proposed distance metric takes into account the intrinsic geometry of the Grassmannian, thus it can preserve more non-linear information of monitoring signal.

3. Experimental verification and analysis

3.1. Data description

Accelerometers positioned above the crosshead gather vibration data reflecting the operational conditions of the RC. This collected data is utilized for validating the proposed method. The schematic represented in Fig.3 provides a visual depiction of the layout and components of the RC system, including the arrangement of sensors within the setup. The accelerometers are mounted above the crosshead. Within the operational dynamics, an engine is tasked

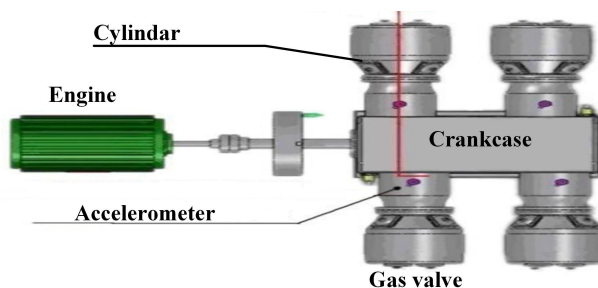


Figure 3: Schematic of RC structure

with furnishing the necessary power to induce rotation in the drive shaft. This rotational motion is facilitated by the reciprocating action of the piston rod, which is orchestrated by the crankshaft. In turn, this reciprocation serves the dual purpose of compressing gas within the cylinder and facilitating the delivery of high-pressure gas. In order to ensure the stable operation and early detection of potential issues, accelerometers are strategically positioned on the crosshead to monitor and analyze vibrations occurring within the cylinder. These sensors act as vital diagnostic tools, providing insights into the mechanical integrity and performance of the system. In the demanding environment of oil refinery plants, a spectrum of common faults can arise, posing challenges to operational efficiency and safety. Among

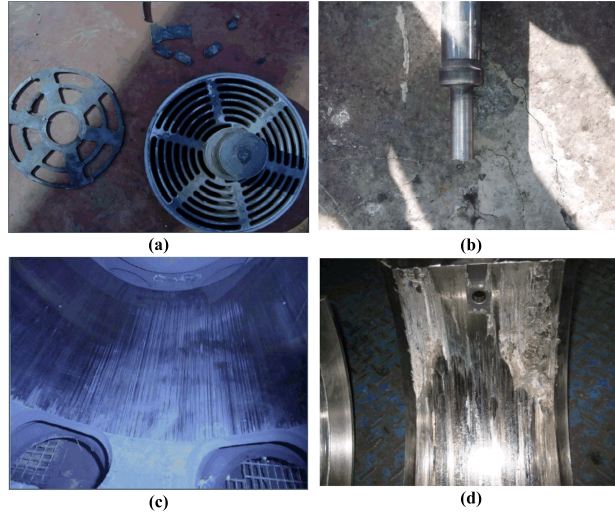


Figure 4: Faults of RC

Table 2: Date description

| Fault type | Description | Rotating speed (rpm) | Sampling frequency (kHz) | Size of training/testing data |
|------------|-----------------------|----------------------|--------------------------|-------------------------------|
| Normal | normal condition | 375 | 12.8 | 200/100 |
| F1 | wear of bearing shell | 375 | 12.8 | 200/100 |
| F2 | cylinder scraping | 375 | 12.8 | 200/100 |
| F3 | gas valve | 375 | 12.8 | 200/100 |
| F4 | piston rod breaking | 375 | 12.8 | 200/100 |

these are gas valve leakages, fractures in the piston rod, instances of cylinder scraping, and wear and tear in bearing shells. Mitigating these issues requires vigilant monitoring, proactive maintenance practices, and swift intervention when anomalies are detected.

Fig.4(a) visually represents a scenario where a gas valve has fractured, resulting in the leak of gas. This issue can have detrimental effects on the operation of the system, potentially leading to safety hazards and operational inefficiencies. In Fig.4(b), the illustration depicts a fractured piston rod which is a common fault observed due to prolonged operation leading to fatigue failure. This type of failure can significantly compromise the functionality of the engine, necessitating immediate attention to prevent further damage and potential system failure. Figs.4(c) and (d) showcase instances of cylinder scraping and the wear of bearing shell, respectively. These faults typically arise from component wear-out and delayed replacement. If left undetected at an early stage, these faults can escalate into more severe operational issues and potentially catastrophic incidents.

Vibration monitoring proves to be a reliable approach for diagnosing faults in the RC. As faults occur, vibrations undergo noticeable changes, making them a valuable indicator for fault detection. In this study, vibration signals were gathered to validate the proposed method. Detailed descriptions of the fault data can be found in Table 2.

To gauge the effectiveness of the developed method comprehensively, its performance was scrutinized across five distinct operating conditions. These conditions were meticulously designed and maintained at a consistent rotating speed of 375 rounds per minute (rpm), ensuring a standardized testing environment. Each operating condition was carefully sampled at a frequency of 12.8 kilohertz (kHz). Each dataset comprises 300 signals, with 200 samples randomly designated for training purposes and the remaining samples allocated for testing.

3.2. Validation of the proposed method

To begin the analysis, data preprocessing are performed firstly. The data preprocessing include the remove of abnormal data, such as data collected by faulty sensor, and normalization within the range of [0,1]. Then the EMD

Table 3: Parameter setting of the DBN

| Parameter | Setting |
|---|---------|
| The number of RBMs | 3 |
| The number of input nodes of the 1st RBM | 36 |
| The number of output nodes of the 1st RBM | 30 |
| The number of output nodes of the 2nd RBM | 20 |
| The number of output nodes of the 3rd RBM | 10 |
| Learning rate | 0.05 |
| The number of epochs | 30 |

technique is applied to disassemble the signals into a collection of individual components, namely the IMFs. These IMFs capture the inherent oscillatory modes present within the original signal, allowing for a detailed examination of its underlying dynamics. The outcomes of this decomposition procedure are visually depicted in Fig.5. These visualizations offer valuable insights into the spectral content and temporal dynamics of the signal across different frequency bands, laying the foundation for further analysis and interpretation. From each IMF, a set of four features outlined

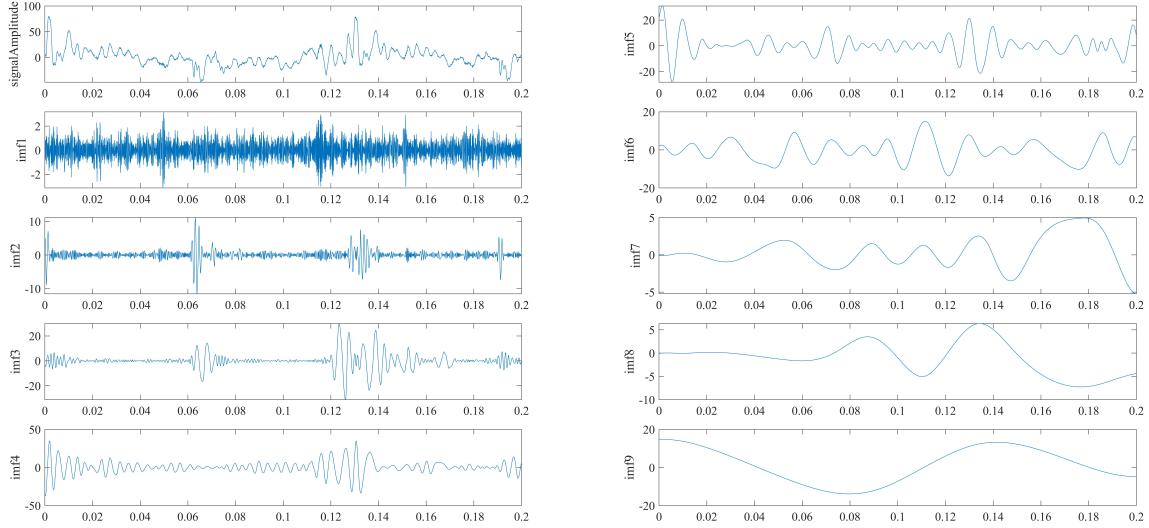


Figure 5: EMD results

in Table 1 is extracted to form a high-dimensional feature vector with a dimensionality of 36. In order to mitigate redundant information and enhance efficiency, these high-dimensional features are inputted into a DBN for feature dimension reduction and deep feature fusion. The network architecture consists of three RBMs, each configured with parameters as specified in Table 3. In the final layer of DBN, there are 10 nodes, yielding a deep fused feature vector with the output dimensionality of 10. This lower-dimensional feature vector encapsulates essential information extracted from the original high-dimensional feature space, facilitating efficient representation and analysis. The initial three components of this deeply fused feature vector are visually depicted in Fig. 6. In this visualization, distinct colors are utilized to denote features corresponding to different operating conditions. This representation provides a clear and intuitive visualization of the feature space, enabling the discernment of underlying patterns and relationships among the features extracted from the input signals.

Subsequently, robust subspaces are established on the Grassmann manifold from the deeply fused feature to discern the type of fault present. The effectiveness of the developed approach is thoroughly assessed on the typical RC fault data, with the diagnostic performance depicted in Fig.7 via the confusion matrix. The x -axis and y -axis respec-

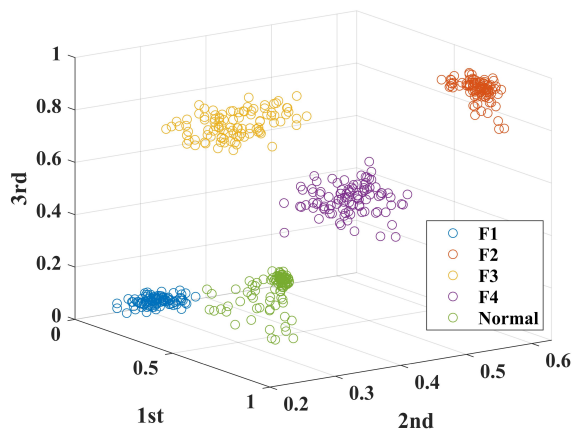


Figure 6: DBN feature visualization

| Predicted Fault | F1 | F2 | F3 | F4 | Normal |
|-----------------|--------|--------|--------|--------|--------|
| F1 | 86.60% | 1.20% | 0.00% | 10.40% | 1.00% |
| F2 | 8.40% | 84.20% | 8.00% | 2.00% | 2.10% |
| F3 | 4.80% | 0.80% | 85.50% | 0.00% | 5.80% |
| F4 | 0.00% | 5.50% | 2.10% | 87.60% | 3.90% |
| Normal | 0.20% | 8.30% | 4.40% | 0.00% | 87.20% |

Figure 7: Confusion matrix

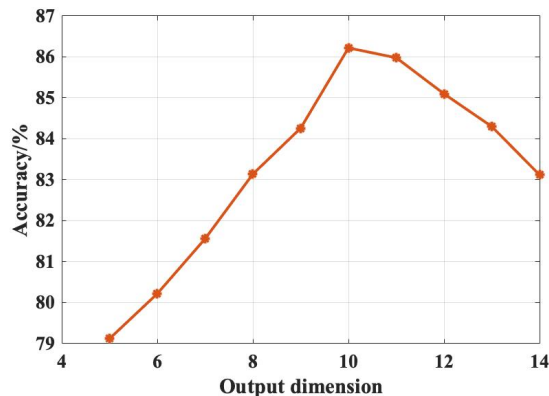


Figure 8: The relationship between output dimension and accuracy

tively indicate the ground-truth and prediction of fault. Within the matrix, the numbers enclosed in yellow squares signify the accuracies of fault diagnosis for each specific fault, while those within green squares denote the detailed misclassification ratios for each fault. Notably, the proposed method achieves impressive fault identification accuracies: 86.6% for fault F1, 84.2% for fault F2, 85.5% for fault F3, 87.6% for fault F4, and 87.2% for normal conditions. It should be noted that the diagnosis accuracies in the paper are the calculated average of ten trials to ensure the stability of final results.

3.3. Parameter analysis and method evaluation

This part investigates the optimal dimensionality for feature fusion within the DBN final layer. Fig.8 visually depicts the correlation between the dimension for feature fusion and the corresponding diagnosis performance. This figure reveals a notable trend: as the output dimension increases, diagnosis accuracies show an improvement, reaching the maximum at 86.22% when the dimension reaches ten. However, beyond this threshold, the accuracy begins to diminish. This suggests that lower-dimensional features encapsulate the most pertinent information, particularly evident at a dimension of ten. Beyond this point, the inclusion of additional dimensions introduces redundant information, thereby adversely impacting the performance of the method.

A comparative study with alternative approaches is carried out across three pivotal regards: feature extraction methods, feature fusion and dimension reduction methods, and fault recognition methods. The summarized compar-

Table 4: Method evaluation

| Method | | | | F1 | F2 | F3 | F4 | Normal |
|--------|--------------|---------------------|------------------------|------|------|------|------|--------|
| Number | Feature type | Dimension reduction | Feature identification | | | | | |
| 1 | features | - | GM | 72.3 | 70.8 | 71.5 | 69.3 | 70.2 |
| 2 | EMD+features | - | GM | 75.6 | 74.2 | 74.6 | 76.6 | 79.3 |
| 3 | EMD+features | KPCA | GM | 82.2 | 83.5 | 82.4 | 84.9 | 84.3 |
| 4 | EMD+features | DBN | SVM | 85.8 | 83.6 | 83.5 | 85.8 | 86.6 |
| 5 | EMD+features | DBN | GM | 86.6 | 84.2 | 85.5 | 87.6 | 87.2 |

Table 5: Method evaluation

| Number | Method | F1 | F2 | F3 | F5 | Normal |
|--------|-------------|------|------|------|------|--------|
| 1 | SVMFE [29] | 72.8 | 79.9 | 80.0 | 77.8 | 84.1 |
| 2 | 1D-CNN [30] | 83.3 | 81.8 | 80.2 | 86.6 | 84.5 |
| 3 | Proposed | 86.6 | 84.2 | 85.5 | 87.6 | 87.2 |

ative outcomes are presented in Table 4. In method 1, features are extracted directly from the original time-series signals. However, this approach exhibits subpar performance in practical applications due to its limited ability to capture nuanced variations in the data. Contrastingly, method 2 leverages EMD to refine inherent vibration signals by multiple IMFs, thereby enhancing diagnosis performance by capturing more localized operating condition characteristics. This approach enables the extraction of essential features from the decomposed IMFs, obtaining improved discriminative power and diagnostic accuracy compared to Method 1. Methods 3, 4 and 5 are compared to demonstrate the effectiveness of deep feature fusion and dimension reduction techniques. Remarkably, Method 5 showcases superior performance in comparison to method 3. This outcome underscores the effectiveness of DBN in seamlessly integrating features while retaining valuable non-linear information that is often overlooked by conventional methods. Furthermore, method 5 outperforms method 4, indicating that the GM-based geodesic distance can effectively retain more reliable information of nonlinearity in feature classification; the intrinsic geometric structure captured by GM contributes significantly to the enhancement of fault diagnosis accuracy.

The proposed method is compared with other state-of-the-art methods to illustrate its superiority. The comparison results are listed in Table 5. As shown in the table, the proposed method outperforms the other methods, achieving an accuracy of approximately 86.22% across four types of faults. In comparison, SVMFE and 1D-CNN achieve 78.92% and 83.28% accuracy, respectively. The 1D-CNN method performs fault diagnosis using differential pressure and differential temperature signals, which are cleaner than vibration signals that often contain significant noise interference. Cleaner signals make it easier to identify regular patterns. However, the effectiveness of 1D-CNN is compromised in RC fault diagnosis when dealing with noisy vibration signals. Similarly, the effectiveness of SVMFE is also compromised. This is likely because SVMFE is particularly suited for diagnosing gas valve faults, where the impulse present in the signal is minimal. When handling signals with significant impulsive features, the performance of SVMFE decreases.

4. Conclusion

The proposed methodology integrates intrinsic oscillation features extracted via EMD, deep feature fusion and dimension reduction using DBN, and assesses similarity on the Grassmann manifold for fault diagnosis in the RC.

EMD method is adopted in the application. It can effectively separates intrinsic oscillation modes, providing localized insights into the RC's dynamics.

Features are extracted from each IMF and constructed into high-dimensional vectors, then DBN are used to produce a lower-dimensional, deeply-fused feature vector. It preserves non-linear information and enhances discriminative capability.

The fused features are mapped onto subspaces on the Grassmann manifold. Geodesic distance is calculated to compare test data with fault data, retaining nuanced information about nonlinearity and improving fault identification accuracy.

Validation with RC fault data from an oil refinery demonstrated the method's effectiveness in refining localized information and deeply fusing features, providing a comprehensive understanding of RC system behavior and fault characteristics. Additionally, this method can be extended to diesel engine fault diagnosis.

Future research will consider feature correlation at different time steps to further enhance RC fault diagnosis performance.

References

- [1] Y. Zhang, J. Ji, B. Ma, Fault diagnosis of reciprocating compressor using a novel ensemble empirical mode decomposition-convolutional deep belief network, *Measurement* 156 (2020) 107619.
- [2] Z. Fan, R. X. Gao, Q. He, Y. Huang, T. Jiang, Z. Peng, L. Thévenaz, Y. Xiong, S. Zhong, et al., New sensing technologies for monitoring machinery, structures, and manufacturing processes, *Journal of Dynamics, Monitoring and Diagnostics* (2023) 69–88.
- [3] Y. Lei, B. Yang, X. Jiang, F. Jia, N. Li, A. K. Nandi, Applications of machine learning to machine fault diagnosis: A review and roadmap, *Mechanical Systems and Signal Processing* 138 (2020) 106587.
- [4] T. Han, W. Xie, Z. Pei, Semi-supervised adversarial discriminative learning approach for intelligent fault diagnosis of wind turbine, *Information Sciences* 648 (2023) 119496.
- [5] P. Jieyang, A. Kimmig, W. Dongkun, Z. Niu, F. Zhi, W. Jiahai, X. Liu, J. Ovtcharova, A systematic review of data-driven approaches to fault diagnosis and early warning, *Journal of Intelligent Manufacturing* 34 (8) (2023) 3277–3304.
- [6] D. Zhang, Z. Feng, Wind turbine planetary gearbox fault diagnosis via proportion-extracting synchrosqueezing chirplet transform, *Journal of Dynamics, Monitoring and Diagnostics* 2 (3) (2023) 177–182.
- [7] X. Wen, Z. Xu, Wind turbine fault diagnosis based on relieff-pca and dnn, *Expert Systems with Applications* 178 (2021) 115016.
- [8] Z. Haiyang, W. Jindong, J. Lee, L. Ying, A compound interpolation envelope local mean decomposition and its application for fault diagnosis of reciprocating compressors, *Mechanical Systems and Signal Processing* 110 (2018) 273–295.
- [9] D. Helm, M. Timusk, Wavelet denoising applied to hardware redundant systems for rolling element bearing fault detection, *Journal of Dynamics, Monitoring and Diagnostics* (2023) 102–114.
- [10] Y. Niu, J. Fei, Y. Li, D. Wu, A novel fault diagnosis method based on emd, cyclostationary, sk and tptsr, *Journal of Mechanical Science and Technology* 34 (2020) 1925–1935.
- [11] J. Li, D. Deng, J. Zhao, D. Cai, W. Hu, M. Zhang, Q. Huang, A novel hybrid short-term load forecasting method of smart grid using mlr and lstm neural network, *IEEE Transactions on Industrial Informatics* (2020).
- [12] R. Sadeghi, H. Samet, T. Ghanbari, Detection of stator short-circuit faults in induction motors using the concept of instantaneous frequency, *IEEE Transactions on Industrial Informatics* 15 (8) (2018) 4506–4515.
- [13] L. Feng, X. Zhang, B. Liu, A high-dimensional spatial rank test for two-sample location problems, *Computational Statistics & Data Analysis* 144 (2020) 106889.
- [14] K. Zhang, B. Tang, L. Deng, X. Yu, Fault detection of wind turbines by subspace reconstruction-based robust kernel principal component analysis, *IEEE Transactions on Instrumentation and Measurement* 70 (2021) 1–11.
- [15] H. Wang, J. Xu, R. Yan, Intelligent fault diagnosis for planetary gearbox using transferable deep q network under variable conditions with small training data, *Journal of Dynamics, Monitoring and Diagnostics* (2023) 30–41.
- [16] G. Jiang, D. Li, K. Feng, Y. Li, J. Zheng, Q. Ni, H. Li, Rolling bearing fault diagnosis based on convolutional capsule network, *Journal of Dynamics, Monitoring and Diagnostics* (2023) 275–289.
- [17] M. Gao, X. He, L. Chen, T. Liu, J. Zhang, A. Zhou, Learning vertex representations for bipartite networks, *IEEE Transactions on Knowledge and Data Engineering* (2020).
- [18] Z. Jin, D. He, Z. Wei, Intelligent fault diagnosis of train axle box bearing based on parameter optimization vmd and improved dbn, *Engineering Applications of Artificial Intelligence* 110 (2022) 104713.
- [19] Q. Li, R. Ma, M. Liao, X. Jing, A novel fault evaluation method based on nonlinear vibration features and euclidean distance measurement for grid-like structures, *Structural Health Monitoring* 22 (6) (2023) 4131–4148.
- [20] S. Boluki, M. S. Esfahani, X. Qian, E. R. Dougherty, Constructing pathway-based priors within a gaussian mixture model for bayesian regression and classification, *IEEE/ACM transactions on computational biology and bioinformatics* 16 (2) (2017) 524–537.
- [21] Z. Fang, W. Wang, Y. Cao, Q. Li, Y. Lin, T. Li, D. Wu, S. Wu, Reciprocating compressors intelligent fault diagnosis under multiple operating conditions based on adaptive variable scale morphological filter, *Measurement* 224 (2024) 113778.
- [22] W. Rong, E. Zhuo, H. Peng, J. Chen, H. Wang, C. Han, H. Cai, Learning a consensus affinity matrix for multi-view clustering via subspaces merging on grassmann manifold, *Information Sciences* 547 (2021) 68–87.
- [23] L. S. Souza, N. Sogi, B. B. Gatto, T. Kobayashi, K. Fukui, Grassmannian learning mutual subspace method for image set recognition, *Neurocomputing* 517 (2023) 20–33.
- [24] Y. Sun, S. Li, X. Wang, Bearing fault diagnosis based on emd and improved chebyshev distance in sdp image, *Measurement* 176 (2021) 109100.
- [25] Y. Wang, Z. Pan, X. Yuan, C. Yang, W. Gui, A novel deep learning based fault diagnosis approach for chemical process with extended deep belief network, *ISA transactions* 96 (2020) 457–467.
- [26] M. Z. Uddin, M. M. Hassan, A. Almogren, A. Alamri, M. Alrubaian, G. Fortino, Facial expression recognition utilizing local direction-based robust features and deep belief network, *IEEE Access* 5 (2017) 4525–4536.
- [27] X. Wang, J. Zhao, A complex process fault diagnosis method based on manifold distribution adaptation, *Engineering Applications of Artificial Intelligence* 87 (2020) 103267.
- [28] L. Xu, S. Chatterton, P. Pennacchi, Rolling element bearing diagnosis based on singular value decomposition and composite squared envelope spectrum, *Mechanical Systems and Signal Processing* 148 (2021) 107174.

- [29] L. Chun-Hui, X. Guo-Lin, Z. Hai-Yang, Z. Hai-Feng, M. Yong-Cai, Fault diagnosis method of reciprocating compressor valves based on svmfe, *Noise and Vibration Control* 42 (5) (2022) 128.
- [30] F.-y. Guo, Y.-c. Zhang, Y. Wang, P. Wang, P.-j. Ren, R. Guo, X.-Y. Wang, et al., Fault detection of reciprocating compressor valve based on one-dimensional convolutional neural network, *Mathematical Problems in Engineering* 2020 (2020).